COBEM 2023 27TH INTERNATIONAL CONGRESS OF MECHANICAL ENGENEERING

ABCM Brazilian Society of Mechanical Sciences and Engineering
27th ABCM International Congress of Mechanical Engineering
December 04-08, 2023, Florianópolis-SC, Brazil

COB-2023-0382
PRELIMINARY AERODYNAMICS ANALYSIS OF A THREE-DIMENSIONAL BUMP AT SUBSONIC AND SUPERSONIC FLOW

John J Vaca-Rios
Hernán Cerón-Muñoz
Department of Aeronautical Engineering, São Carlos Engineering School, University of São Paulo, Area 2. Avenida João Dagnone, no 1100 - Jardim Santa Angelina, São Carlos 13563-120, São Paulo, Brazil.
jjvacar@usp.br
hernan@sc.usp.br

Abstract. *A three-dimensional compression surface (bump) is used in the inlet system of an aircraft engine to compress the incoming airflow and reduce the boundary layer that is built up over the fuselage. In this paper, both the subsonic and supersonic flow patterns over a bump are studied numerically. The bump is modeled using the Stream Tracing Technique, and it is located on a long flat plate to simulate a typical forebody flow. A three-dimensional structured mesh with eight blocks is generated by using ICEM, a meshing Computational Fluid Dynamics (CFD) software. The Reynolds Averaged Navier-Stokes equations are solved using the ANSYS Fluent code with the turbulence model k-ε. The density-based method with the implicit scheme is used for both the supersonic and subsonic cases. The grid sensitivity tests are performed by using bias and grid refinements in the block edges, perpendicular to the walls, and varying the number of elements from* 0.5 *to* 8 *million. The results proved that the current bump on supersonic conditions efficiently diverts the boundary layer. In the aerodynamics analysis of the bump flow field, it was found that the spanwise pressure gradient on the bump has a corresponding relationship with the diversion of the boundary layer. The supersonic flight conditions presented a decrease in the total pressure recovery in comparison with the subsonic ones due to the total pressure losses caused by the thickening of the boundary layer, the supersonic flow compression from the shock wave formation, and the existence of shock boundary layer interaction (SBLI) in the supersonic flight conditions. It may be concluded that, due to its acceptable aerodynamic performance, the current bump is an appropriate candidate for integration into a forebody in order to carry out a future aerodynamic analysis of an inlet system.*

Keywords: *bump, diversion, shock boundary layer interaction, Computational Fluid Dynamics (CFD)*

1. INTRODUCTION

A supersonic fighter equipped with a jet engine should be capable of keeping its performance for a wide range of the flight envelope i.e. different Mach, altitudes, angle of attack, etc. On the other hand, a supersonic inlet as the first component of the propulsion system, should be designed to provide the required air flow with an acceptable level of energy (high-pressure recovery), quality (low distortion), and reduced minimum drag (Mattingly *et al.*, 2006; Askari and Soltani, 2019).

Supersonic external compression is generated by a combination of an oblique shock wave (in a single-stage or multistage manner, depending on the aircraft velocity) and a normal shock wave formed on the compression surface, known as the shock system (Ferri and Nucci, 1951). The inlets are designed in such a way that, when operating in the vicinity of their design point, these shock waves impinge at a point on their cowl lip, called an impingment point. This condition is known as the Shock on Lip (SOL) condition and can be seen in Figure 1b. Such a condition, which is known as the critical operating condition for the external compression type inlets, results in a maximum inlet mass flow and a minimum spillage drag.

For an operating case where the inlet back-pressure is higher than the corresponding value during the critical operating condition, the inlet normal shock wave moves upstream significantly (see Figure 1c), increasing the mass flow spillage. Such a condition is known as a subcritical operating condition and severe shock boundary layer interaction (SBLI) usually occurs on the supersonic compression regions. In this case, the supersonic inlet experiences shock wave oscillations and a consequent flow instability known as the inlet buzz (Chen *et al.*, 2017; Farahani *et al.*, 2019).

In contrast, if the inlet back pressure becomes lower than the value during the critical operating condition, the inlet throat will choke, the internal flow after the throat becomes supersonic and a secondary normal shock would be formed in the inlet diffuser. This inlet condition is known as the supercritical operating condition and is shown in Figure 1a. Considering an actual flight, an aircraft encounters various flight conditions where the impingment point might occur away from the cowl lip. In such a situation, variable structures are usually used to adjust the inlet geometry to recover the SOL condition.

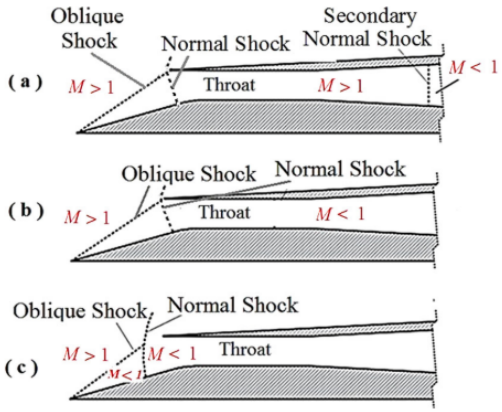

Figure 1. Supersonic inlet various operating conditions. (Abedi *et al.*, 2020).

Supersonic inlets are designed and integrated on aircraft in various configurations and classifications such as supersonic flow compression region, flow dimensions, installation position, etc. The supersonic inlets can be classified according to i) the region where take place the compression, ii) flow dimensions, and iii) the fuselage location. The supersonic inlet has allowed the evolution and adaptation of the newer propulsive system; they have been developed, designed, built, tested, failed, succeeded, moved, bled, swept, twisted, and adapted to meet even more challenging requirements and speed regimes (Scharnhorst, 2012). Yet still operate and maneuver efficiently at subsonic speeds (i.e., takeoff and landing regimes).

All the supersonic inlets must comply with general requirements such as mechanical, environmental, and of course aerodynamics (Scharnhorst, 2012). Some of the supersonic inlets use mechanisms that can generate additional weight and may increase drag. In contrast, the Diverterless Supersonic Inlet (DSI) does not require additional mechanisms and if well designed could generate less drag than other supersonic inlets. The mechanical simplicity and acceptable aerodynamic performance with lower weight made DSI the first choice of Lockheed Martin designers of the F-35 Lightning II (B Saheby *et al.*, 2020).

The DSI is a type of inlet that consists of a 3D bumped surface at the start of inlet and a forward swept inlet cowl. Figure 2 shows a 3D bump. The bumped surface acts as a compression surface on the surface of the fuselage. This bump creates a high-pressure zone effectively pushing the boundary layer away from the inlet. The inlet cowl lip is generally forward swept which also helps in effective diversion of the boundary layer. Due to its ability to effectively divert the boundary layer, the DSI usually does not contain a diverter and a bleed or bypass system. The removal of these movables parts not only reduces the complexity of inlet structure but also decreases the aircraft's weight by about 30%, cost of production, and maintenance challenges (Hehs, 2000). The bump inlet is also seen to perform better in supersonic Mach regimes (Halwas and Aggarwal, 2019), though one option for improving its performance in subsonic regimes would be to use adaptive bump (Zhao *et al.*, 2022). Due to the compression surface in front of the inlet, several compression waves are formed and the final shockwave is considerably weak in front of the inlet. This gives higher total pressure recovery inside the air inlet.

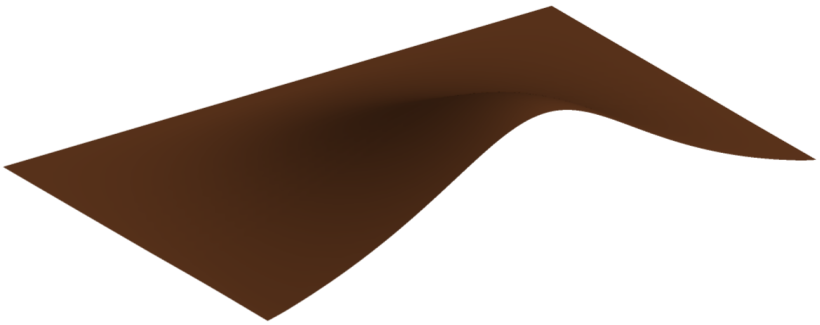

Figure 2. A 3D bump.

The bump surface at the start of DSI also provides a shielding effect of the engine fan blade against detecting signals, significantly reducing the radar cross section (RCS) of the aircraft (Mufti *et al.*, 2019; Xu *et al.*, 2017). Some modern fighter aircraft including DSI are the Chengdu J-10B/C, CAC/PAC JF-17 Thunder, Chengdu J-20 and Lockheed Martin

F-35 Lightning II. The DSI significantly enhances the operational performance of the aircraft on which it is integrated.

Diverterless supersonic inlet integration for a flight vehicle requires a three-dimensional compression surface (bump) design with an acceptable shock structure and boundary layer diversion; this results in a low drag induction system with acceptable propulsive efficiency (B Saheby *et al.*, 2020). The DSI is formed on the basis of a fuselage-integrated dual-purpose bump compression surface which diverts the upstream boundary layer in addition to compressing the air for the inlet.

An interesting result about the bump diversion percentage is presented in Xu *et al.* (2017). With the compute of boundary layer thickness in four points over the bump, it can be seen in the points near to bump top that the boundary layer thickness was less than the thickness in the bump outer points. This behavior was observed for all the numerical experiments. This means that there exists a transversal pressure gradient that displaces the boundary layer regardless of geometry used. A detailed study reveals that a long bump with a smooth beginning and end has better results than a blunt bump (Svensson, 2008). That for subsonic and supersonic Mach numbers as well as high Mach numbers, as observe in Arif *et al.* (2017).

It is the position of the bump relative to the inlet that it is advantageous to place the maximum amplitude of the bump close to the cowl lips of the intake so that they coincide with the shock from the bump surface (Svensson, 2008). The same result was reached in B Saheby *et al.* (2020). It is important to control at the same time other bump parameters such as length, width, and height because they affect the pressure recovery in the longitudinal direction. Especially where the bump starts, because there exists a shock wave whose strength varies with those parameters and consequently modified the pressure recovery coefficient.

A computer analysis was carried out in the present work to examine the performance of a bump in diverts a boundary layer. The section 2 describes the methodology implemented. This section includes details about the computational domain and the boundary conditions in subsection 2.1. Subsection 2.2 covers all the important issues about both grid generation and its evaluation. The solver setup is briefly described in subsection 2.3. Section 3 discusses the results in terms of boundary layer height, Mach contours, and total pressure contours. Conclusions are drawn in the last section.

2. METHODOLOGY

2.1 Computational domain and boundary conditions

As can be seen in Fig. 3, it was considered only half domain to reduce the computational time in solver stages. The domain length, width, and height are $10L$, $1L$, and $1L$, respectively. The bump's total length (L) is $1m$ but the present study was carried out with a bump cut at its maximum height, at location $x/L = 0.64$. At the inlet and top boundaries were specified the appropriate Mach number with Pressure Far-Field type boundary condition. The bottom boundary represents an aircraft fuselage, then as well as the bump, it was treated as no slip and adiabatic wall. The two sides of the domain were symmetry and the outlet was configured as Pressure Outlet type with zero gauge pressure.

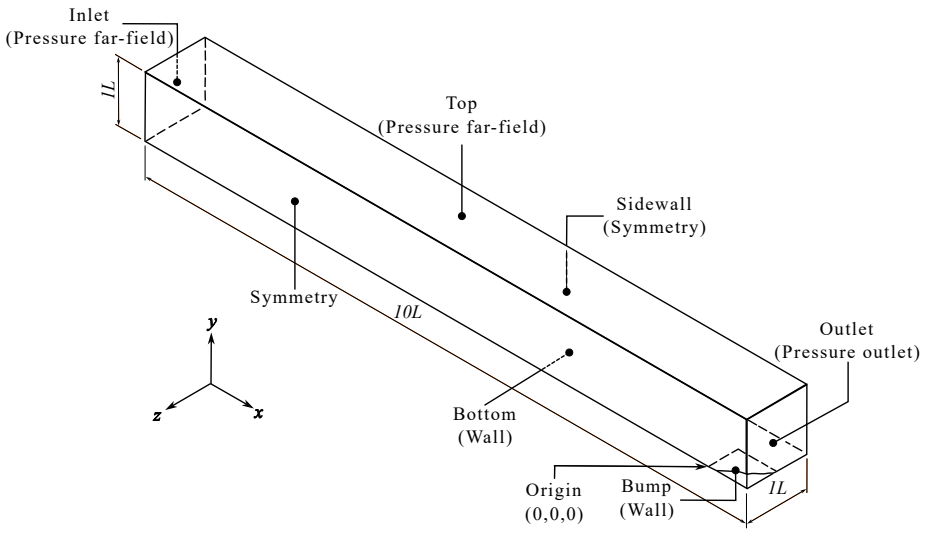

Figure 3. Computational domain.

2.2 Grid generation

Multiblock structural grids were generated on the computational domain for simulation on the present three dimensional geometry. The total number of cells varies from 0.5 to 8 million cells. The mesh is concentrated in the regions surrounding the long flat plate and bump surfaces, and using the exponential mesh law with a $3.32097 \times 10^{-6} m$ height for the first cell. For the coarser grid, the first cell height is $5.1630 \times 10^{-3} m$ and used the uniform mesh law. The growth of the mesh was controlled with proper *size linking* between adjacent blocks. Figure 4 shows details of the structured mesh used for the present 3D simulations. For the supersonic flow regimes studied is expected that appear the SBLI phenomenon, because of this, the boundary layer must be captured adequately. y^+ values were ≈ 1 on the entire surface for matching that requirement. A mesh sensitivity study was performed with four meshes and for high-speed supersonic flow. As shown in Tab. 1 Total Pressure Recovery (TPR) and Flow Distortion (FD) were selected as sensitivity criteria.

Total pressure recovery was calculated with the Eq. 1 and flow distortion with the Eq. 2.

$$TPR = \frac{avg.(P_{o,e})}{P_{o,\infty}}, \tag{1}$$

where $avg.(P_{o,e})$ is the average total pressure at outlet boundary and $P_{o,\infty}$ the freestream total pressure.

$$FD = \frac{max(P_{o,e}) - min(P_{o,e})}{avg.(P_{o,e})} \tag{2}$$

The percentage changes both for TPR and for FD between the 6.0×10^6 and 8.4×10^6 grids were less than 3%, then the 6 million cells grid was selected for the present study.

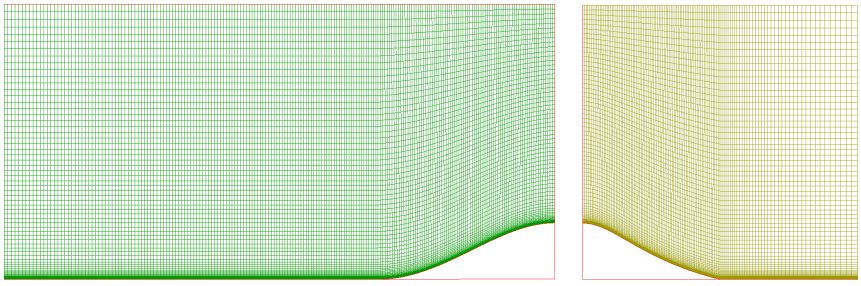

(a) $xy-$ plane. (b) $yz-$ plane.

Figure 4. Surface mesh cut view.

Table 1. Mesh sensitivity analysis.

Cells$\times 10^6$	**TPR**	**TPR change [%]**	**FD**	**FD change [%]**
0.5	0.978	-	1.049	-
4.3	0.454	-53.58	2.242	113.73
6.0	0.488	7.49	2.059	-8.16
8.4	0.475	-2.66	2.109	2.43

2.3 Solver

The Reynolds Averaged Navier-Stokes equations were solved using the ANSYS Fluent code with the turbulence model k-ε. The density-based method with the implicit scheme was used for both the supersonic and subsonic cases. Convective fluxes were discretized with AUSM (Advection Upstream Splitting Method) scheme. The spatial discretization was performed with third order MUSCL (Monotone Upstream-Centered Schemes for Conservation Laws) for flow values at the face cell. The Least Squares Cell Based discretization was employed to estimate the gradient of quantities at the face cell. The Courant number was 0.5 to improve the convergence of the solution. All the residuals were set up as 1.0×10^{-4}. Each simulation was run with 20000 iterations and took an average of 48 PC hours. Simulations were run on a PC with a 2.5 GHz Intel Xeon CPU E5-2670 processor, 128 GB memory, and Windows 10 Pro Operating System.

3. RESULTS

To analyze the results, a parallel plane was drawn to the yz plane and located $10mm$ before the outlet boundary. At the intersection of that plane with the surface of the bump, five control points were located in the z direction. Three of those points were on the bump, one on the border between the bump and the flat plate, and another on the flat plate. This last point was located in $2z/W = 1.5$. The points were named symmetry, one-third, two-thirds, bottom, and undisturbed respectively.

According to Fig. 5a the shock wave angle for the bump (β_b) was $43°$. The shock wave on the bump was weaker than the theoretical shock wave on a $20°$ wedge and stronger than the theoretical shock wave on a $20°$ cone. From the exact solution, the shock wave angle for a wedge (β_w) is $53°$, and for a cone (β_c) is $37°$. The Fig. 5b shows the shock wave cone over the bump, its geometry is important for the future design of the engine inlet cowl lip. The shock wave cone seems to be detached, maybe because of SBLI that slightly shifts the impingement point to the left. The boundary layer near the bump's leading edge is laminar, but it is turbulent close to the trailing edge. The velocity profiles close to the outlet can be seen in Fig. 6. The velocity profiles in the symmetry and one-third lines look like turbulent boundary layers. A typical laminar boundary layer behavior is appreciated in the three left lines, that is in the transverse direction. To obtain the velocity profiles of Fig. 6, inviscid simulations were made to calculate the edge boundary layer velocity u_e of each analyzed point. The dimensionless boundary layer thickness was calculated with the output boundary layer thickness as the reference value (i.e., δ_o).

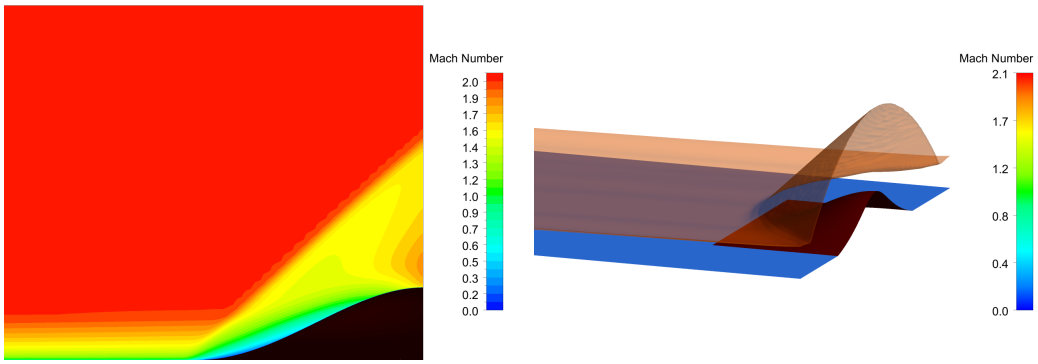

(a) Mach contour at $2z/W = 0$. (b) Mach cone.

Figure 5. Case $M = 2.0$.

For the supersonic cases, as shown in Fig. 7, the thickness of the boundary layer on the symmetry point is lower than that of the undisturbed one, and the thickness of the boundary layer at the bottom of the bump is higher than that of the undisturbed field on the analysis plane. It signifies that the device redirects the boundary layer attached to the bump to the bottom point. That is, the bump causes displacement in the boundary layer.

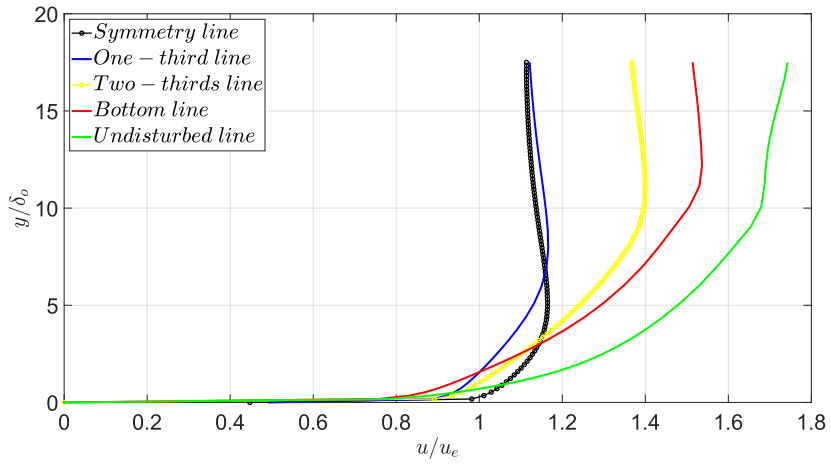

Figure 6. Velocity profiles for $M = 2.0$.

The transverse pressure gradient is slight near the outlet of the bump, as can be seen tracking the pressure over the

horizontal line on pressure contour in Fig. 7. It can be seen that for $M = 2.0$ the streamwise pressure gradient over the bump is higher than for $M = 1.6$. The maximum location of the total pressure is $\approx 50mm$ upstream of the outlet and over the symmetry plane. As a result, it is assumed that the bump has a matching relationship between the boundary layer displacement and the transverse pressure gradient on the bump. When boundary layer low energy fluid travels along the bump, the low energy fluid is deflected to both sides. The reason for this is that the pressure gradient acts as a lateral force on the fluid on the bump, causing the flow, particularly the boundary layer, to be diverted to two sides of the bump. Another observation is that the pressure contour for $M = 1.6$ is more dispersed than for $M = 2.0$, this causes a low pressure gradient in almost all regions except behind the highest pressure point. Behind this point, both cases are qualitatively similar.

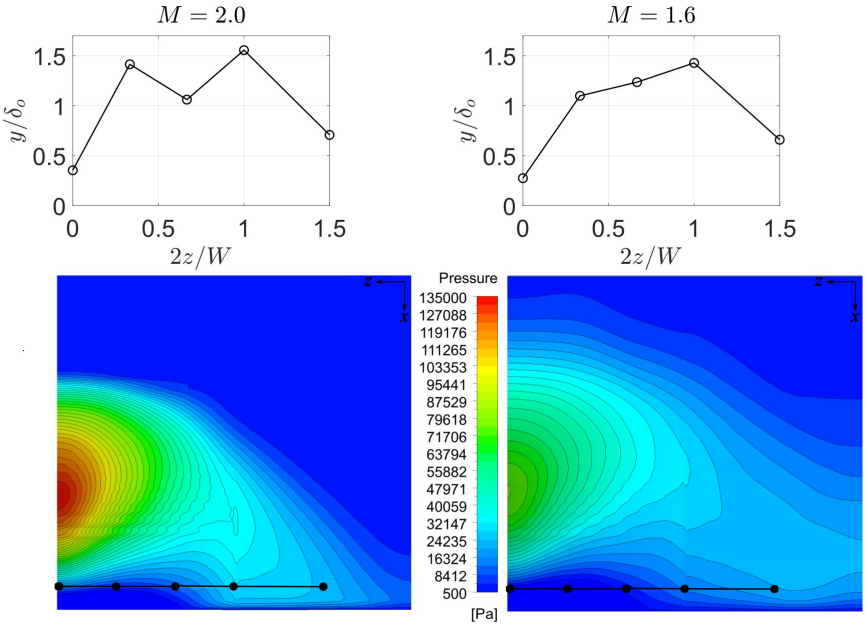

Figure 7. Transverse boundary layer and pressure gradient.

The thickness of the boundary layer in the subsonic regime is less than in the supersonic simulations, as shown in Fig. 8, and the displacement of the boundary layer occurs towards the two-thirds line. It has also been discovered that decreasing the Mach number reduces the displacement of the boundary layer. Taking these observations into account, if the bump were used in a Diverterless Supersonic Inlet, it is expected that the latter would have a lower performance in the subsonic regime than in the supersonic one.

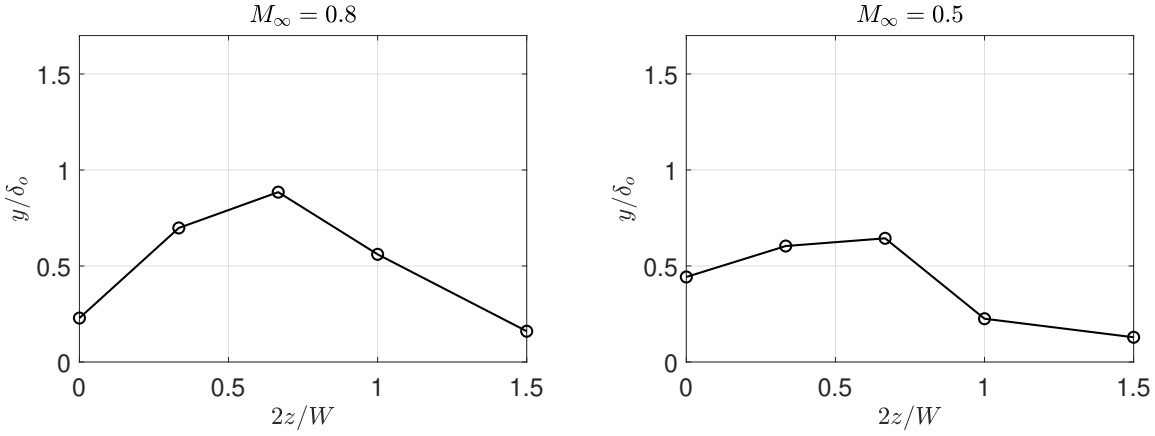

Figure 8. Transverse boundary layer.

4. CONCLUSION

Numerical testing was conducted on a bump located on a long flat plate. The present tests were performed at subsonic and supersonic regimes. At $x/L = 0.63$ the results showed the bump diverts the boundary layer toward its borders for supersonic cases and toward the two-thirds line for subsonic cases. If the bump were used in a Diverterless Supersonic Inlet, preliminary results showed that the design Mach number would be near 1.6 because, at this Mach number, the boundary layer ingestion would be less than at $M = 2.0$ case, i.e., transverse boundary layer thickness for $M = 1.6$ are less than the corresponding thickness for $M = 2.0$. As a result, the bump's fixed design has proved satisfactory performance throughout a rather broad range of Mach numbers without the use of moveable structural pieces or an auxiliary flow control mechanism.

5. ACKNOWLEDGEMENTS

The authors would like to thank the Department of Aeronautical Engineering (EESC/USP) for their availability of laboratories and we also would like to thank all the support given by colleagues. This work was funded in part by the Conselho Nacional de Desenvolvimento Científico e Tecnológico - Brasil (CNPq) under grant number 141271/2020-5.

6. REFERENCES

Abedi, M., Askari, R., Sepahi-Younsi, J. and Soltani, M., 2020. "Axisymmetric and three-dimensional flow simulation of a mixed compression supersonic air inlet". *Propulsion and Power Research*, Vol. 9, No. 1, pp. 51–61.

Arif, I., Ahmed, M., Salamat, S. and Ghafoor, M., 2017. "Flow field analysis of different intake bump (compression surface) configurations on a supersonic aircraft". In *7th international conference on advances in engineering and technology (AET-17), Phuket, TH*. pp. 25–26.

Askari, R. and Soltani, M., 2019. "Effects of mach number on the performance of a diverterless supersonic inlet". *Journal of Aircraft*, Vol. 56, No. 4, pp. 1697–1707.

B Saheby, E., Shen, X. and Hays, A.P., 2020. "Design and performance study of a parametric diverterless supersonic inlet". *Proceedings of the Institution of Mechanical Engineers, Part G: Journal of Aerospace Engineering*, Vol. 234, No. 2, pp. 470–489.

Chen, H., Tan, H.J., Zhang, Q.F. and Zhang, Y., 2017. "Buzz flows in an external-compression inlet with partially isentropic compression". *AIAA Journal*, Vol. 55, No. 12, pp. 4286–4295.

Farahani, M., Daliri, A. and Younsi, J.S., 2019. "Supersonic inlet buzz detection using pressure measurement on wind tunnel wall". *Aerospace Science and Technology*, Vol. 86, pp. 782–793.

Ferri, A. and Nucci, L.M., 1951. "Preliminary investigation of a new type of supersonic inlet". Technical report, NATIONAL AERONAUTICS AND SPACE ADMINISTRATION HAMPTON VA LANGLEY RESEARCH CENTER.

Halwas, H.K. and Aggarwal, S., 2019. "Effect of side gust on performance of external compression supersonic inlet". *Journal of Aircraft*, Vol. 56, No. 2, pp. 569–582.

Hehs, E., 2000. "Diverterless supersonic inlet". *Code One Magazine*, Vol. 15, No. 3, p. 8–13.

Mattingly, J.D., Boyer, K.M. and von Ohain, H., 2006. *Elements of propulsion: gas turbines and rockets*. American Institute of Aeronautics and Astronautics Reston, VA.

Mufti, B., Khan, T., Masud, J. and Toor, Z., 2019. "Flow field analysis of a diverterless supersonic inlet using embedded les methodology". In *2019 IEEE 10th International Conference on Mechanical and Aerospace Engineering (ICMAE)*. IEEE, pp. 79–84.

Scharnhorst, R., 2012. "An overview of military aircraft supersonic inlet aerodynamics". In *50th AIAA Aerospace Sciences Meeting Including the New Horizons Forum and Aerospace Exposition*. p. 13.

Svensson, M., 2008. *A CFD Investigation of a Generic Bump and its Application to a Diverterless Supersonic Inlet*.

Xu, S., Wang, Y., Wang, Z. and Fan, X., 2017. "The design and analysis of bump in high speed supersonic flow". In *21st AIAA international space planes and hypersonics technologies conference*. p. 2269.

Zhao, C., Zhou, L. and Qiu, T., 2022. "Research on flexible skin technique for adaptive bump inlet structure". *Aircraft Engineering and Aerospace Technology*.

7. RESPONSIBILITY NOTICE

The current authors are solely responsible for the printed material included in this paper.